Particle Accelerators, 1995, Vol. 48, pp. 213–237
Reprints available directly from the publisher
Photocopying permitted by license only

ANALYSIS OF METHODS FOR CONTROLLING MULTIBUNCH INSTABILITIES IN DAΦNE

S. BARTALUCCI,* M. BASSETTI,* R. BONI,* S. DE SANTIS,† A. DRAGO,* A. GALLO,* A. GHIGO,* M. MIGLIORATI,* L. PALUMBO,*† R. PARODI,# M. SERIO,* B. SPATARO,* G. VIGNOLA,* and M. ZOBOV*

* *INFN–Laboratori Nazionali di Frascati, C.P. 13, 00044 Frascati, Italy*

† *Dip. di Energetica, Universita' La Sapienza, Roma, Italy*

INFN–Sezione di Genova, Via Dodecaneso 33, 16146 Genova, Italy

(Received 5 November 1993; in final form 3 August 1994)

The e^-e^+ DAΦNE collider is designed to reach a luminosity of the order of $10^{32}-10^{33}$ sec^{-1} cm^{-2} at 510 MeV, by storing high current. Such a current, few amperes per beam, can in principle be achieved by filling many RF buckets in the machine. One of the main beam dynamics problems concerns the multibunch instabilities caused by the strong coupling between the beam and the parasitic higher-order mode (HOM) resonances of the RF cavity. Due to the high current, the instability is very fast, so it is impossible to stabilize the beam with a feedback system alone. An effort has to be made to reduce the shunt impedance of the cavity HOMs so that a feedback system can be effective. This task is accomplished by properly designing the RF cavity and by coupling out the HOMs through loops or wave-guides to extract energy from the resonant fields, thus reducing at the same time the quality factor Q and the shunt impedance R. The residual excitation of beam oscillations is damped by a bunch-by-bunch digital feedback system.

KEY WORDS: Collective effects, impedances, instabilities, storage rings

DEFINITIONS OF SYMBOLS USED IN THIS PAPER

α_c	Momentum compaction.
α_1	Dipole oscillations growth rate $(1/\tau_1)$.
α_{eff}	Effective dipole oscillations growth rate $(1/\tau_{\text{eff}})$.
α_f	HOM filling rate.
a_{fb}	Feedback damping rate.
β	Natural angular frequency for a single HOM.
ΔE	Energy deviation.

ΔU_{fb}	Feedback energy correction.
$\Delta\varphi$	Phase angle of synchrotron oscillations.
e	Electron charge.
E	Nominal electron energy.
$\mathbf{E}_w(\mathbf{r})$	Waveguide electric field.
$\mathbf{G}_m(\mathbf{r}, \mathbf{r}')$	Magnetic Green function for a rectangular waveguide (3×3 matrix).
$g_o(\tau)$	Stationary longitudinal phase space distribution.
h	Harmonic number.
$\mathbf{H}_o(\mathbf{r})$	Cavity unperturbed magnetic field.
$\mathbf{H}_w(\mathbf{r})$	Waveguide magnetic field.
$i(t)$	Induced wake current in the inductance of a single HOM.
$i_b(t)$	Beam current.
I_o	Beam average current.
I_m	Beam current amplitude of m^{th} harmonic.
$\mathbf{J}_s(\mathbf{r})$	Current density.
$J_m(x)$	Bessel function of the first kind of m^{th} order.
k_{pm}	HOM loss factor.
k_b	Number of bunches.
n	Relative oscillation mode number.
P_n	Single mode dissipated power.
P_T	Total dissipated HOM power.
P_w	Total power dissipated in the waveguide loads.
Q	Cavity quality factor.
q_b	Bunch charge.
R	Cavity shunt resistance.
σ_t	RMS bunch duration.
τ	Longitudinal phase space amplitude.
τ_f	HOM filling time.
τ_1	Dipole rise time.
τ_d	Longitudinal radiation damping time.
τ_{eff}	Effective dipole rise time.
$\bar{\tau}_{\mathrm{eff}}$	Asymptotic effective rise time (for high Q).
τ_n	Damping time of the energy of the n^{th} HOM.
T_b	Time distance between two adjacent bunches.
U	Total energy of a single HOM.
U_{bb}	Energy loss for the broad band impedance.

U_o Energy loss by radiation for the synchronous particle.

U_r Energy loss by radiation.

$v(t)$ Induced wake voltage for a single HOM.

V_g Generator voltage.

$Z(\omega)$ HOM impedance.

ω_o Revolution angular frequency.

ω_c Coherent synchrotron angular frequency.

ω_r Resonance angular frequency for a single HOM.

ω_s Incoherent synchrotron angular frequency.

1 INTRODUCTION.

In the Φ-Factory DAΦNE,[1] a 510 MeV e^+e^- twin-ring collider under construction at Frascati Laboratories (see Table 1), the luminosity goal is achievable by storing a high current in many bunches. This has required a strong effort on the study of the control of multibunch instabilities. The instability problem can be addressed both by reducing the causes and by applying cures.

Analysis of the interaction of the beam spectrum with the parasitic modes of the RF cavity shows that the instability growth rates depend on the strength of the "stable" and "unstable" sidebands and their position with respect to the HOMs.[2,3]

TABLE 1: DAΦNE single ring parameter list.

Machine length	97.69	(m)
Revolution freq.	3.069	(MHz)
RF frequency	368.26	(MHz)
Harmonic number	120	
Number of Bunches	$30 \div 120$	
V_{RF}	254	(KV)
Energy	510	(MeV)
Radiation loss/turn	9.32	(KeV)
Momentum compaction	$5.8*10^{-3}$	
Synchrotron frequency	22.88	(KHz)
RMS bunch duration	100	(psec)
Longitudinal damping time	17.8	(msec)

For HOMs with very high Qs, it is really unlikely that a sideband couples to an HOM. The shunt impedance of these HOMs also is very high, but is harmless as long as the HOM is not excited by a sideband. Unfortunately, the HOM frequency can drift during machine operation because of thermal excursions or as a side effect of tuning the fundamental mode, leading to a strong coupling and very fast instability.[4,5]

A careful design of the cavity shape can lead to HOMs with rather low shunt impedances $R/Q < 1\ \Omega$, but these values are not low enough to maintain stability in the case of full coupling.

Recent development of HOM damping techniques have shown that, for normal-conducting cavities, it is possible to achieve Qs less than 100, thereby obtaining a strong reduction of the beam-HOM coupling.[6–8] This would make it possible to damp the residual multibunch instabilities by means of a feedback system.[9–13]

This paper describes the results obtained at the design stage for DAΦNE. In Section 2 the theoretical estimates of the growth rates are presented. The optimum design of an RF cavity with low HOM content is briefly described in Section 3. The HOM damping techniques, which have been investigated, are treated in Section 4. Section 5 illustrates the bunch-by-bunch feedback system. The time domain simulation code, which is able to show the beam dynamics behavior and the effectiveness of the feedback system, is described in Section 6.

2 THEORETICAL GROWTH RATES

2.1 Coherent frequency shift

The analysis of the dynamics of k_b equally spaced bunches interacting with the long-range wake fields is performed by computing the coherent frequency shift predicted by Sacherer's theory.[2]

The spectrum of the bunches executing free dipole oscillations exhibits lines at angular frequencies

$$\omega_p = (pk_b + n)\omega_o + \omega_s \tag{1}$$

$$-\infty < p < +\infty, \quad 0 \leq n \leq k_b - 1, \quad p, n \text{ integers},$$

where n is the number of the relative mode of oscillation and ω_s the synchrotron angular frequency.

In DAΦNE, due to the high revolution frequency, the unstable sidebands corresponding to a given n, are quite far apart. A single HOM with high Q can at most excite a single sideband. For a damped HOM, with $Q \approx 100$, the resonator can significantly couple to a few unstable sidebands. However, the bandwidth is such that, apart from $n \approx k_b/2$, there will not be compensation of stable and unstable sidebands.

In the following analysis we consider the effect of a single HOM coupling to the relative bunch motion n. Let ω_r, R and Q be the resonator parameters. In this simple case the coherent frequency shift is[3]

$$j(\omega_c - \omega_s) = \frac{\theta_1(q)}{q} Z(q\omega_o + \omega_c) I_o \ , \tag{2}$$

with

$$\theta_1(q) = -\frac{\alpha_c}{\omega_s(E/e)} \int_o^\infty \frac{\partial g_o}{\partial \tau} J_1^2(q\omega_o \tau) d\tau \ , \tag{3}$$

where I_o is the beam current, α_c the momentum compaction, $q = pk_b + n$, $Z(q\omega_o + \omega_c)$ the resonator impedance, and $g_o(\tau)$ the stationary phase space distribution.

In the realistic case $\omega_c \ll \omega_r$, the impedance can be approximated by:

$$Z(q\omega_o + \omega_c) \approx \frac{R}{1 + \frac{j\omega_c}{\alpha_f} + jtg(\Phi_r)} \ , \tag{4}$$

where

$$\alpha_f = \frac{\omega_r}{2Q} \quad \text{and} \quad tg(\Phi_r) = Q\left(\frac{q\omega_o}{\omega_r} - \frac{\omega_r}{q\omega_o}\right) \tag{5}$$

are the filling rate of the resonant mode ($\tau_f = 1/\alpha_f$ = filling time) and the detuning of the resonant mode with respect to the line q of the bunch spectrum, respectively.

The coherent tune shift is obtained by solving the following equation:

$$\omega_c^2 + \left[\alpha_f tg(\Phi_r) - \omega_s - j\alpha_f\right]\omega_c - \alpha_f\left[\omega_s tg(\Phi_r) - \frac{\theta_1(q)RI_o}{q} - j\omega_s\right] = 0. \tag{6}$$

The customary way of computing the coherent frequency shift[4,5] considers the bunch spectrum at angular frequencies ω_p, i.e., the spectrum of a bunch with dipole perturbation executing free oscillations in the absence of growth or damping. Once the impedance spectrum is known, this procedure leads to the solution for the unknown ω_c. This is not exactly what is prescribed in Equation (2), where the impedance has to be computed at the shifted frequencies. As a matter of fact, Equation (2) is an eigenvalue problem for ω_c. Computing the impedance at the bunch spectrum sidebands (1) leads to an estimate of the growth rates that is not exact, especially in the case of high Q resonances.[14,15]

2.2 *Dipole mode, on resonance*

Assuming a resonator at $\omega_r = q\omega_o + \omega_c$, we get:

$$\omega_c = \omega_s + j\frac{\alpha_f}{2}\left[1 - \sqrt{1 + 4\frac{\theta_1(q)RI_o}{q\alpha_f}}\right] . \tag{7}$$

As expected, in the full coupling condition there is no real shift of the synchrotron frequency, whereas the imaginary shift gives the growth rate of the instability. We recognize in the term

$$\frac{q}{\theta_1(q)RI_o} = \tau_1 \tag{8}$$

the instability rise time usually obtained from Equation (2).

It is interesting to analyze two different regimes.

For $\tau_1 \gg \tau_f$, we get

$$\omega_c \approx \omega_s - j\frac{1}{\tau_1} . \tag{9}$$

In this case the rise time given by Equation (8) can be considered a fairly good approximation.

Quite different results are obtained in the other case, namely when $\tau_1 \ll \tau_f$, for which we get:

$$\omega_c \approx \omega_s - \frac{j}{\sqrt{\tau_1 \tau_f}} . \tag{10}$$

The effective rise time $\tau_{\text{eff}} = \sqrt{\tau_1 \tau_f}$ is the geometric mean of τ_1 and τ_f. One could conclude from the above equation that cavities characterized by an extremely long filling time should be preferred from the standpoint of the multibunch instabilities. Using the explicit expression of the two terms in the rise time of Equation (10), we have:

$$\tau_{\text{eff}} = \left(\frac{2q}{\theta_1(q)\omega_r I_o(R/Q)}\right)^{\frac{1}{2}} . \tag{11}$$

Therefore, in the regime $\tau_1 \ll \tau_f$ the effective rise time is inversely proportional to the square root of the ratio R/Q. By increasing Q and keeping R/Q constant, the effective rise time reaches an asymptotic value and is no longer dependent on the cavity filling time.

As an example we plot in Figure 1, as a function of Q, the growth rates $\alpha_1 = 1/\tau_1$ and $\alpha_{\text{eff}} = 1/\tau_{\text{eff}}$ computed for DAΦNE. The plot assumes a parasitic resonance with $R/Q = 1\Omega$, at $\omega_r = 500\omega_o + \omega_s$, exciting the motion of 30 bunches of 3 cm RMS length for a total current of 1.4 A. The upper curve is the growth rate $\alpha_1(Q)$ while the lower one is $\alpha_{\text{eff}}(Q)$. Note that at high Qs the difference between the two curves becomes larger and larger. To verify the correctness of Equation (7), we show on the same plots the instability growth rates (dots) obtained from the time domain simulation code[16] described in Section 6. The numerical results agree quite well with those computed from Equation (7).

For the DAΦNE cavity, only a few undamped HOMs with a relatively high shunt impedance give a τ_{eff} significantly higher than τ_1. In Table 2 we show the results relative to the HOMs of the DAΦNE cavity given by URMEL.[17] The rise times computed with Equation (7) are given for $\omega_p = \omega_r$ (on resonance). Analogous results for the measured HOMs of the cavity prototype are shown in Table 3. One can see that when the HOM beats on resonance, the instability is extremely fast and incurable, whereas for damped HOMs the rise time is much longer and easily curable with a feedback system.

It must be said that Landau damping could noticeably affect the instability once the HOMs have been damped. In Figure 2 we show the Q required for the 0-MM-1[a] cavity mode versus

[a] We follow the HOM nomenclature as given by the URMEL code.

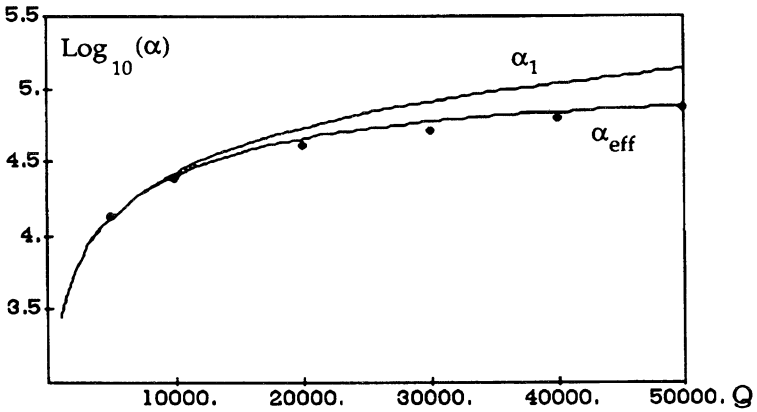

FIGURE 1: Growth rates $\alpha_1(Q)$ and $\alpha_{\rm eff}(Q)$, for an HOM with R/Q=1Ω.

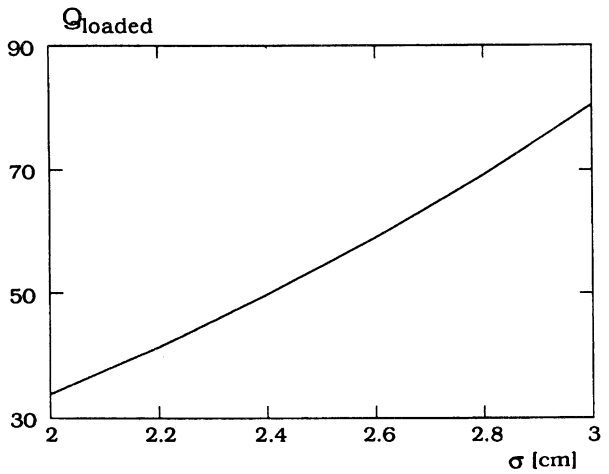

FIGURE 2: Q_L vs. bunch length for 0-MM-1 Landau stability.

the bunch length. The damping time depends almost on the square of the bunch length, and for bunches shorter than 3 cm, much stronger damping of the HOM would be required. Moreover, the real coherent shift could make it ineffective.

For the sake of completeness, we point out that the growth rates have been worked out assuming an individual coupling of one sideband with a single resonator. These calculations neglect the superposition of the shunt impedance of several HOMs on the same relative mode. This effect can enhance the coupling (sum of shunt impedances) or reduce it (difference of shunt impedances). The time simulation code shows that for DAΦNE these effects are generally negligible, even in the presence of the HOM damping system.

TABLE 2: URMEL Monopolar Cavity Modes

MODE TYPE	FREQ. [MHz]	(R/Q) [Ω]	Q_0	$\tau_{\text{eff}}[\mu s]$
0-EM-1	367.38	61.38	49100	
0-MM-1	695.97	15.81	49800	8
0-EM-2	794.85	0.01	81900	1850
0-MM-2	987.18	0.01	65900	2100
0-EM-3	1069.79	0.25	66900	96
0-EM-4	1119.92	2.11	57500	20
0-MM-3	1138.40	0.09	56800	270
0-EM-5	1203.83	0.79	67600	37
0-MM-4	1283.84	0.17	56200	150
0-EM-6	1318.43	0.77	72400	35
0-MM-5	1390.57	0.33	57800	81
0-EM-8	1481.07	0.85	55400	38
0-MM-7	1570.06	0.55	62200	51
0-EM-9	1574.96	0.88	61000	35
0-EM-10	1665.50	0.17	68200	136
0-MM-8	1672.18	1.12	63100	29
0-MM-9	1717.68	0.22	68500	109
0-EM-11	1742.33	0.21	57300	133
0-MM-10	1774.36	1.53	62400	24
0-EM-12	1796.49	0.13	56400	217
0-MM-11	1866.16	0.47	63300	62
0-EM-14	1955.71	0.15	91400	133
0-EM-15	2011.62	0.23	59500	132
0-MM-13	2038.39	0.24	64400	120

2.3 Some considerations regarding high Q cavities

The shortest rise time given by the "on resonance" asymptotic value of τ_{eff}, which we call $\bar{\tau}_{\text{eff}}$, is reached for $\tau_f \gg \tau_1$, i.e., for HOMs characterized by very high Qs. It might happen that the machine parameters are such that $\bar{\tau}_{\text{eff}} > \tau_d$ (damping time).

Therefore, at the design stage, it is interesting to compare the effective rise time $\bar{\tau}_{\text{eff}}$ with the damping time τ_d due to radiation effect or to the Landau damping. If $\bar{\tau}_{\text{eff}} > \tau_d$, the beam is stable without any changes to the RF cavity. As an example we give the condition for a beam stabilized by the radiation damping.

TABLE 3: Measured modes of the cavity prototype

MODE	UNLOADED MODES				LOADED MODES			
	Freq. [MHz]	R/Q [Ω]	Q_0	τ_{eff} [μs]	Freq. [MHz]	Q_L, Calc.	Q_L, Meas.	τ_{eff} [ms]
0-EM-1	357	61	25000		349.5		22000	
0-MM-1	747.5	16	24000	9	745.7	75	70	1.37
0-EM-2	796.8	0.5	40000	90	796.5	550	230	12.9
0-MM-2	1023.6	0.9	28000	60	1024.9	190	150	10.0
0-EM-3	1121.1	0.3	12000	370	1125.4	–	240	18.3
0-MM-3	1175.9	0.6	5000	440	1172.0	65	100	21.9
0-EM-4	1201.5	0.2	9000	730	1194.3	220	130	50.5
0-EM-5	1369.0	2.0	5000	135	1361.6	115	300	2.2
0-MM-4	1431.7	1.0	2000	670	1423.2	–	750	1.8
0-EM-6	1465.0	0.1	2000	6670	1467.6	–	190	71.2

For short Gaussian bunches, it is useful to write down the effective rise time in the form

$$\bar{\tau}_{\text{eff}} = \left(\frac{4(E/e)\omega_s}{I_o\alpha_c}\right)^{\frac{1}{2}} \frac{1}{\omega_r(R/Q)^{\frac{1}{2}}} \,. \tag{12}$$

The condition $\tau_1 \ll \tau_f$ requires that

$$Q\sqrt{R/Q} \gg \sqrt{\frac{\omega_s(E/e)}{I_o\alpha_c}} \,, \tag{13}$$

and $\bar{\tau}_{\text{eff}} > \tau_d$ gives

$$\omega_r\sqrt{R/Q} < \omega_o(U_o/e)\sqrt{\frac{\omega_s}{\pi^2 I_o\alpha_c(E/e)}} \,. \tag{14}$$

The two relations above are never fulfilled in DAΦNE. However, for typical R/Q values, the conditions are better satisfied for superconducting cavities at very high energy, provided that the momentum compaction is very small.

3 A CAVITY WITH LOW HOM IMPEDANCES

RF power requirements are not highly demanding in a storage ring like DAΦNE. At the operating energy of 510 MeV and a beam current of 1.4 A in 30 bunches, a peak voltage

up to 250 kV is required in the RF cavity, mainly to control the bunch length. The power dissipation in the cavity has to be kept reasonably low to ease the mechanical and cooling design. A shunt resistance as low as $R = 2M\Omega(V^2/2P)$ for the fundamental mode seems acceptable. This enables us to consider the minimization of the R/Q for the HOMs as the main goal of the design process in order to reduce the beam cavity coupling.

3.1 HOM power loss

The total energy U_t delivered to the cavity HOMs by the passage of a bunch is given by:

$$U_t = \sum_{\text{all the HOMs}} U_n = \sum_n \frac{1}{2}\omega_n (R/Q)_n \exp\left(-\omega_n^2 \sigma_t^2\right) q_b^2 = k_{pm} q_b^2 , \tag{15}$$

where U_n, ω_n and $(R/Q)_n$ are, respectively, the energy, the resonant angular frequency and the ratio between the shunt resistance and quality factor of the n^{th} HOM; q_b is the bunch charge; σ_t is the bunch rms time duration, and k_{pm} is the cavity HOM loss factor.

The energy of the n^{th} cavity HOM U_n decays exponentially with a time constant $\tau_n = Q_n/\omega_n$. If τ_n is much smaller than the time distance between adjacent bunches T_b, the mode dissipates the power $P_n = U_n/T_b$. However, this is the case only for modes that are very heavily damped. For most modes, the fields induced by a bunch passage survive long enough to interact with the following bunches and the total power dissipated has to be calculated in the frequency domain.

The beam current can be expressed as a Fourier series:

$$i_b(t) = \sum_{m=-\infty}^{+\infty} I_m \exp\left[jm\omega_o t\right] . \tag{16}$$

The total HOM power depends strongly on the cavity monopole spectrum and increases when the beam lines I_m overlap the cavity spectrum. Such a power can be calculated as follows:

$$P_T = \sum_{m=o}^{+\infty} \sum_{\text{all the HOMs}} \frac{2(R/Q)QI_m^2}{1 + Q^2\left(\frac{m\omega_o}{\omega_r} - \frac{\omega_r}{m\omega_o}\right)^2} . \tag{17}$$

The probability that a beam spectrum line interacts with the resonator spectrum is very small for an undamped cavity, but if this does happen, the associated power loss can be very high. For a strongly damped cavity, as in our case, the overlap probability is much higher, but the resultant power loss is moderate, with a limit value $P_T = U_t/T_b$.

3.2 Procedure for designing the cavity shape

The basic idea is to "open" the beam tubes at the cavity irises to let the higher-frequency parasitic modes propagate through them,[18] and use tapers as gradual transitions from the cavity iris to the ring vacuum pipe. This implies a strong reduction of both longitudinal and transverse characteristic impedances (R/Q) of all the HOMs, except for the lowest-frequency

ones, which need special care. After a careful analysis of the longitudinal wake potentials by means of the code TBCI,[19] a design with two long tapers was proposed.[20] Comparisons to a conventional design with tubes parallel to the axis and short tapers, showed a significant difference in the loss factor to the HOMs ($k_{pm} = 0.07$ against 0.16 V/pC with a bunch of 3 cm) and a slightly larger value of R/Q at the fundamental-mode. Since the single-pass loss factor for a cavity resonant mode is proportional to the R/Q of the mode, on the average all the R/Qs are decreased substantially. This fact was confirmed by a frequency-domain analysis (by means of the codes OSCAR2D[21] and URMEL), where the presence of some strong HOMs above the beam tube cutoff was observed in the short tapered structure, but not in the long tapered structure. Comparison between the total loss factor and the sum over the resonant modes (15) shows that, for a bunch of 3 cm, less than 10% of the energy loss is due to the high-frequency fields above the beam pipe cutoff.

The final design is quite low in power loss, broad band impedance and resonant impedance.

We have investigated two examples of accelerating cavities: the "bell-shaped" (or "rounded") cavity and the "nose-cone" cavity. In the latter the "nose-cones" are introduced to concentrate the electric field in the region of the beam, thus increasing the R/Q of the fundamental mode. For this geometry, a considerable improvement of the R/Q in the 0-MM-1 mode and a worsening of the transverse mode 1-EM-1 have also been observed. In the high-Q, "rounded" structure, on the other hand, the smooth profile is beneficial for dipole modes but retains a large value for the 0-MM-1 mode, which closely follows the behavior of the accelerating mode.

We found a significant difference only for the first HOM modes as shown in Table 4. In fact for the other HOMs up to cutoff, the behavior of the two cavities is quite similar, as displayed in Figures 3a and 3b.

TABLE 4: Nose-cone vs. Rounded

	Nose-cone	Rounded		Nose-cone	Rounded
Frequency (MHz)	368.3	368.3	0-MM-1 mode:		
R/Q (Ω)	69.9	61.7	Frequency (MHz)	704.7	696.8
Q	34000	49000	R/Q(Ω)	4.2	16.0
R_s (MΩ)	2.37	3.04	Q	30000	50000
k_l (V/pC)	0.101	0.129	R_s (kΩ)	128	800
k_0 (V/pC)	0.077	0.068	1-EM-1 mode:		
k_{pm} (V/pC)	0.024	0.061	Frequency (MHz)	565.0	532.7
k_t' (V/pC/m)	1.16	1.38	R'/Q(Ω)	30.3	13.7
k_{pm}/k_0	0.31	0.91	Q	42000	54000
k_t'/k_0 *1 mm	0.015	0.020	R_s' (MΩ)	1.28	0.74

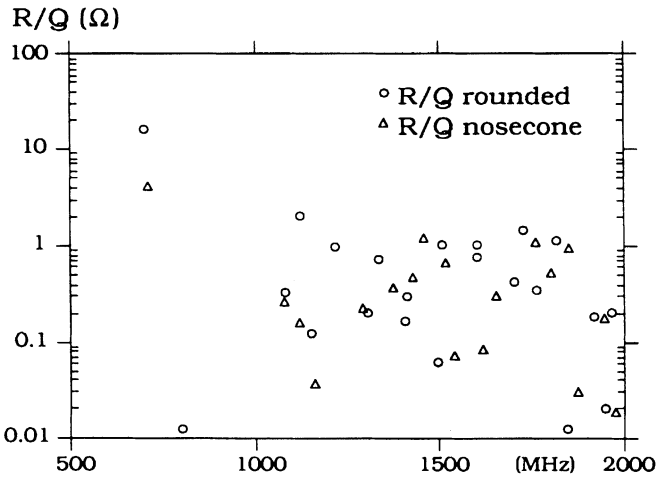

FIGURE 3a: Characteristic impedances of the monopole modes.

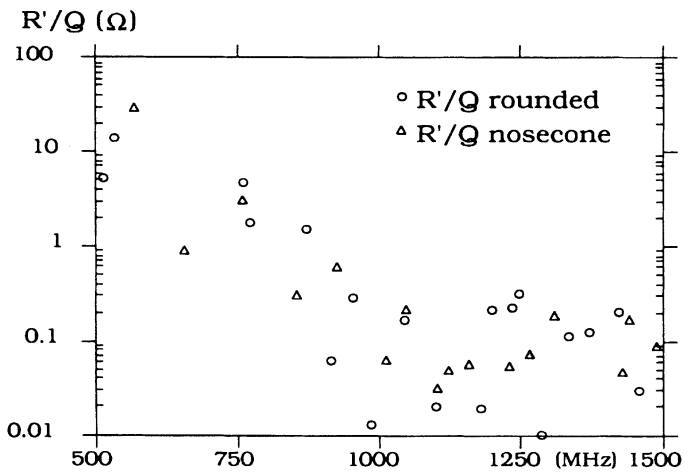

FIGURE 3b: Characteristic impedances of the dipole modes.

Even though the R/Qs are very low, the rise time of the instability could be very fast. Therefore damping of these modes is required. This made the choice of the cavity independent on the particular shape; the rounded cavity was finally chosen for ease of construction.

The final design is shown in Figure 4. Much care has been taken to keep all HOM frequencies far away from harmonics of the bunch repetition rate in order to avoid resonant enhancement of the parasitic power loss.

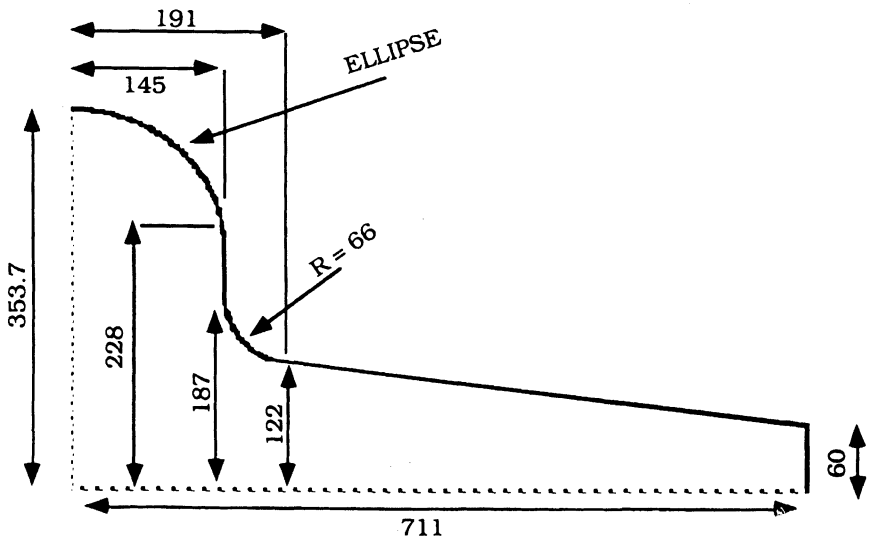

FIGURE 4: DAΦNE cavity shape and dimensions (mm).

4 HOM DAMPING

The problem of parasitic mode damping in room temperature RF accelerating cavities for high-current particle accelerators is being faced in other laboratories[6,22] and the proposed or adopted solutions depend upon the accelerator demands.

A well-known method of damping HOMs consists of coupling them out of the cavity by means of loops or antennas that are applied to the resonator surface in correspondence of the peaks of the parasitic fields and dissipating the extracted power on external 50 Ω loads through coaxial lines. As a rule, the transmission response of such devices must vanish at the cavity fundamental frequency in order to avoid extracting the accelerating field energy; therefore they require some kind of tuning. The effectiveness of a loop/antenna coupler in damping a specific cavity mode can be excellent if its response has a maximum at the mode frequency.

HOM coupling can also be achieved by opening slots onto the cavity surface and conveying the fields out with waveguides. Energy must then be dissipated by means of high-loss materials applied in the vacuum environment or external loads placed beyond a vacuum separation window. The waveguide being a natural high-pass filter, the accelerating field remains trapped in the cavity, provided that the waveguide cutoff is above the cavity fundamental-mode frequency.

We have applied and tested both damping systems to some cavity models. The results obtained with the waveguides have been more satisfactory due to the wide band waveguide response and their capability to reject the fundamental-mode without any tuning device. We have then considered more practical to use waveguide dampers instead of loops or antennas.

4.1 Waveguide to Cavity HOM coupling

Thus far, the description of the electromagnetic fields in a resonant cavity loaded with impedance-matched waveguides has not been satisfactorily made by existing simulation codes. Therefore, different approximate techniques have been developed to solve the problem. These methods[7,8] allow to work out the most meaningful cavity parameters (such as loaded Q values and beam longitudinal and transverse impedances) starting from the output data of 2D and 3D computer codes.

A general rule to optimize the damping effect is to open the waveguide slots onto the cavity surface where the azimuthal HOM magnetic field H_o has the maximum intensity.

The loaded Q values can be approximately estimated by considering the unperturbed field H_o as source of waves propagating in the waveguide.

The current density source $\mathbf{J}_s(\mathbf{r})$ on the aperture surface S can be derived from the unperturbed magnetic field $\mathbf{H}_o(\mathbf{r})$ as:

$$\mathbf{J}_s(\mathbf{r}) = \mathbf{n} \times \mathbf{H}_o(\mathbf{r}) \quad \text{on the surface } S, \tag{18}$$

where $\mathbf{n}$ is the outward unit vector normal to S.

In a rectangular waveguide, the magnetic field $\mathbf{H}_w(\mathbf{r})$ can be obtained from the well-known magnetic Green's function of the waveguide $\mathbf{G}_m(\mathbf{r}, \mathbf{r}')$[23] as

$$\mathbf{H}_w(\mathbf{r}) = \int_{s'} \mathbf{G}_m(\mathbf{r}, \mathbf{r}')\mathbf{J}_s(\mathbf{r}')d^2\mathbf{r}' \tag{19}$$

The magnetic field $\mathbf{H}_w(\mathbf{r})$ can be expanded in terms of normal modes propagating in the waveguide. As long as the cavity mode has a frequency between the cutoffs of the first and second waveguide modes the sole non-evanescent term in Equation (19) is the TE_{10} waveguide mode. Other expansion terms should be considered for mode frequencies above the second waveguide mode cutoff. Even in this case, due to the symmetry of the source, the term associated with the waveguide TE_{10} mode is the most relevant one in the expansion; thus, we can conclude:

$$\mathbf{H}_w(\mathbf{r}) \approx \mathbf{H}_{\mathrm{TE}_{10}}(\mathbf{r}) \, . \tag{20}$$

Assuming a perfectly matched waveguide, the total energy associated with the Poynting vector is dissipated in the waveguide termination load, i.e.,

$$P_w = \frac{1}{2}\int_{s'} \mathrm{Re}\left[\mathbf{E}_w \times \mathbf{H}_w^*\right] da = \frac{1}{2} Z_{\mathrm{TE}_{10}} \int_{s'} |H_{wt}|^2 \, da \, , \tag{21}$$

where P_w is the power dissipated in the waveguide load, $Z_{\mathrm{TE}_{10}}$ is the waveguide impedance, S' is the waveguide cross section, and H_{wt} is the $\mathbf{H}_w$ transverse component.

Finally, the external Q of the cavity mode due to the loading of several waveguides is given by:

$$Q_{\mathrm{ext}} = \frac{\omega_r U}{\sum_i P_w} \tag{22}$$

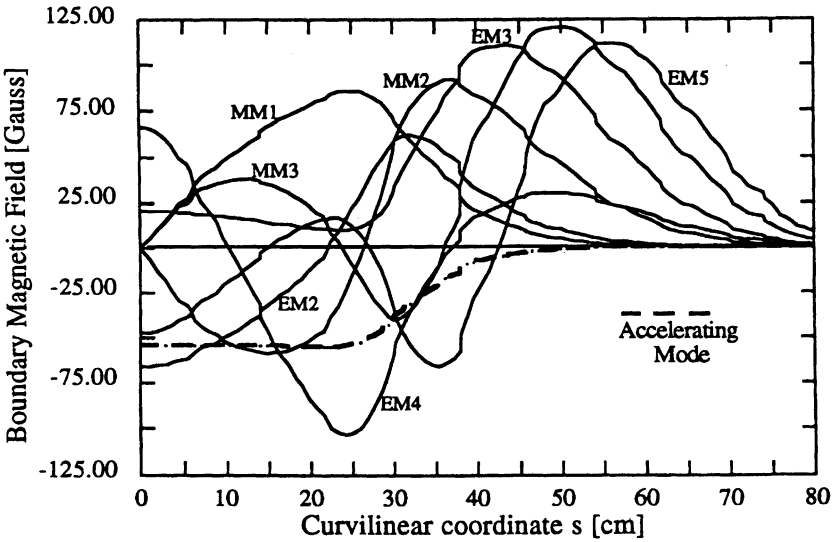

FIGURE 5: Surface field distribution of the cavity modes.

The calculation of Q_{ext} becomes less accurate as the wavelength decreases with respect to the wider slot size. For a wavelength to slot size ratio close to unity, the computed and measured $Q_{\text{ext}} \approx Q_{\text{loaded}}$ values are in the same order of magnitude as shown in Table 3.

4.2 Cavity Damper Design

The surface field has been calculated with the code OSCAR2D as a function of the curvilinear coordinate s of the cavity profile (see Figure 5) for some HOMs. The center of the cell profile is the curvilinear coordinate reference. The highest R/Q mode, 0-MM-1, has its magnetic field peak at $s = 23$ cm; some higher-frequency modes have a maximum in the tapered tubes.

To improve the damping of the 0-MM-1, without perturbing the fundamental-mode symmetry, three waveguides can be applied 120° apart at $s = 23$ cm onto the cavity surface. The waveguide cutoff frequency should be 500 MHz to allow the dipole modes 1-MM-1 and 1-EM-1, at 511 and 532 MHz respectively, to propagate.

Other modes can effectively be coupled by the waveguides, as shown in Figure 5. One more waveguide with a cutoff at 1070 MHz can be located on each tapered tube where some high frequency HOMs penetrate and have magnetic field peaks. The waveguides on tapers can be rotated 90° apart to couple the dipoles also.

4.3 Cavity Prototype Tests

A low power copper cavity model has been manufactured. Due to some mechanical imperfections, the measured frequencies differ slightly from those calculated with the codes,

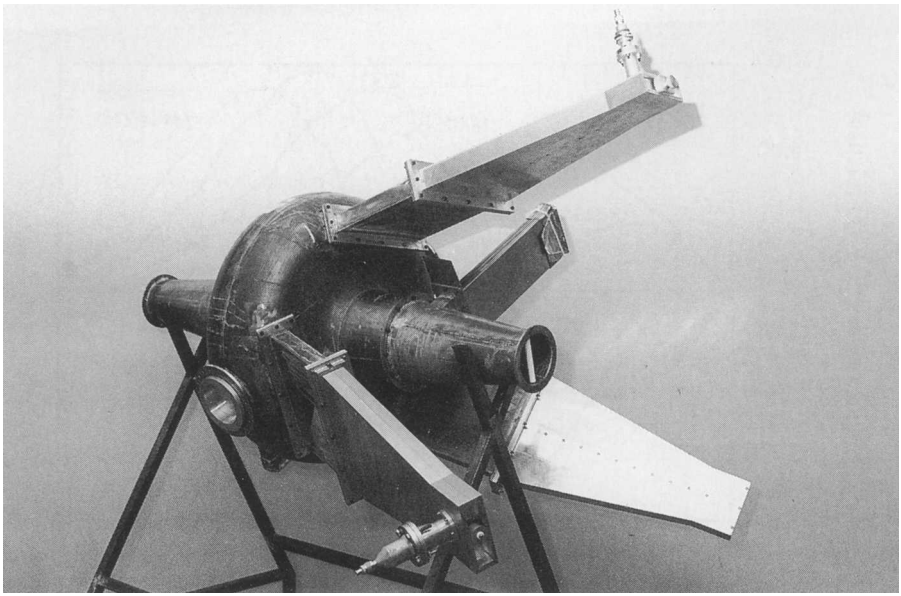

FIGURE 6: The DAΦNE cavity low power model.

but the HOM quality factors were high enough (of order 10^4) to perform reliable damping measurements.

Several kinds of waveguides have been tested on the cavity main body. A rectangular (305×40 mm^2) waveguide has been chosen being the best compromise between high HOM damping and low fundamental-mode degradation.

The waveguides applied to the tapers have a 140×40 mm^2 rectangular cross section and do not degrade the fundamental-mode since that field vanishes at those locations (Figure 6).

A complete characterization up to 1.5 GHz of the cavity prototype fully equipped with waveguides is given in Table 3, together with the analytical estimate of some HOM Qs. The fundamental-mode Q degradation due to the evanescent field in the waveguides is less than 15% and a frequency variation of about -2% has been measured; therefore the outer diameter of the final cavity has been reduced by about 1 cm to get a 2% increase of the unloaded fundamental-mode frequency.

A mechanical sketch of the RF cavity proposed for DAΦNE is shown in Figure. 7. Three additional circular ports in the cavity main body allow insertion of loops or antennas if more damping of particular modes will be needed.

4.4 Waveguide Termination Loads

To estimate the HOM power delivered to the cavity, the measured damped Qs of the cavity model have been considered. The HOM frequencies and R/Qs values were taken from the cavity code simulation. The maximum estimated total power was $P_T \approx 150$ W, corresponding to an asymmetrical machine filling of 27 bunches (instead of 30). The asymmetrical filling is required in order to avoid ion trapping.

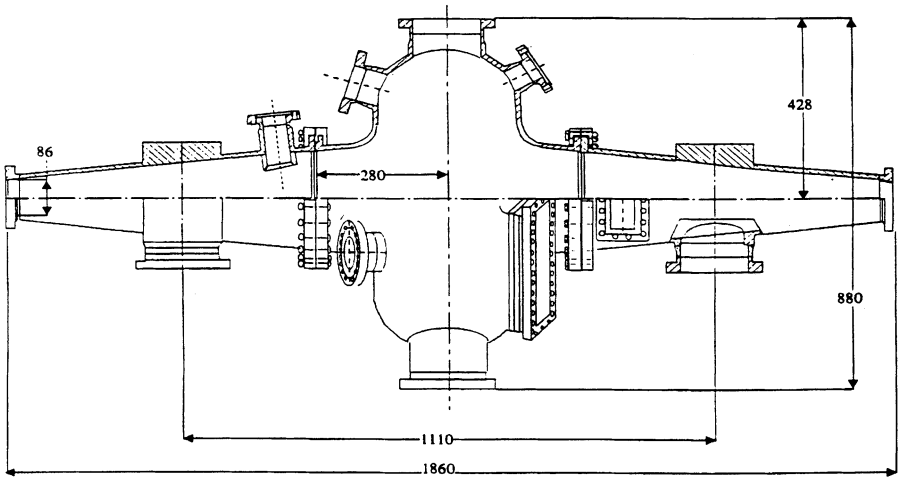

FIGURE 7: Sketch of the DAΦNE cavity.

The power must be dissipated by high-loss material placed either in the ultrahigh vacuum (UHV) or in air after an Al_2O_3 rf window.

Both rf and UHV characteristics of an absorbing material consisting of plain ferrite tiles have been obtained.[24] The results show that the UHV desorption of this material is compatible with the machine vacuum but that the ferrite brazing to the UHV side requires some care.

With an Al_2O_3 RF window the frequency bandwidth could not be wide enough to couple out all the HOM power up to the DAΦNE beam pipe cutoff frequency ($\approx$ 2.5 GHz).

A novel and interesting solution to extract the cavity HOM power is a wideband waveguide-to-coaxial transition that converts the waveguide TE_{10} mode to the TEM mode in a large frequency range ($\approx$ 2.5 octaves) with very low power reflections (VSWR $<$ 2). Such a device, recently developed at LNF,[25] allows the use of commercial coaxial N type or 7/8" ceramic feedthroughs to transfer the RF power to an external 50 Ω load. In this case, the possibility of sampling the HOM beam power with a directional coupler connected to the transition coaxial output, is a very attractive byproduct.

5 BUNCH-BY-BUNCH FEEDBACK

In this section we describe the main features of the damping feedback system adopted for controlling the longitudinal instabilities in DAΦNE.

5.1 The feedback layout

The system proposed for DAΦNE is a bunch-by-bunch, time-domain feedback. This choice is common among multibunch, high-intensity machines.[9]

In a bunch-by-bunch longitudinal feedback system, k_b effective loops act in parallel to damp the synchrotron motion of k_b bunches, treated as individual, independent oscillators. The motion of each bunch is thus effectively decoupled from that of the other bunches independently of the nature of the driving force (e.g., in the presence of an individual perturbation such as an injection error, or in the presence of bunch-to-bunch coupling by HOMs in the RF cavity).

The basic scheme for each effective damping loop is the following. The phase error of the synchrotron oscillation of each bunch is detected with a high-frequency longitudinal pickup, down-converted to base-band and shifted by $\pi/2$ at the synchrotron frequency by means of a proper filter. The resulting signal, which is now in quadrature with the phase oscillation and in phase with the energy oscillation, is amplified and used to impart an energy-correction kick proportional to the instantaneous energy error, by means of a longitudinal kicker. In the smooth approximation the damping rate is:

$$\alpha_{fb} = \frac{1}{4\pi}\omega_o \frac{\Delta U_{fb}}{\Delta E} , \tag{23}$$

where ΔU_{fb} is the energy correction by the feedback kicker and ΔE is the instantaneous energy error.

In order to damp k_b bunches independently of each other, k_b separate filters are necessary. With a maximum number of 120 bunches, this basic approach could become very if not prohibitively complex. The analog/digital technology available today, however, allows considerable simplification.

The proposed system consists of a single front-end phase detector followed by a fast analog to digital converter, capable of digitizing the phase signal of individual bunches at the full rate, with 8-bit resolution. The filtering action is performed numerically by Digital Signal Processor (DSP) chips. Ideally, only one processor, through which all the data are passed, would be needed, but in practice, the data rate is too high and a digital de-multiplexer is used to divide this task between several parallel processing modules, each of which implements the same filter algorithm on different data. The feedback correction information from several parallel processors is multiplexed into a fast digital to analog converter, then amplified with a power amplifier and fed to each bunch at each traversal of the longitudinal kicker.

The number of revolutions encompassed by a synchrotron oscillation is very high, thus an overwhelming number of samples is available to reconstruct a synchrotron oscillation. In order to reduce the complexity of the feedback processing (and the number of DSPs needed), the down-sampling technique is adopted.[10] This consists of processing the detected signal only after a certain number of turns. The last computed correction kick is held in a fast memory register and made available at each bunch passage until a new correction is computed.

5.2 *Front end*

We need to measure the single bunch error with a phase detector but the use of a tuned detector, is precluded because any signal feed-through by the preceding bunches must be avoided.

The bunch signal from a longitudinal pick up is fed to a microstrip comb generator[11] in which a coherent burst of bipolar pulses is produced. The phase of this pseudo-sinusoidal signal with respect to the RF voltage is measured by means of a double-balanced mixer in which the local oscillator is a harmonic of the ring radio-frequency.

The phase detector output goes into a fast digitizer (input bandwidth 1.2 GHz) capable of sampling with 8-bit resolution at 500 Msample/sec.

5.3 *Digital filter*

A demultiplexer distributes the digitized bunch signal to the proper DSP, which performs the filtering algorithm, producing the feedback correction. This correction signal is calculated by a Finite Impulse Response (FIR) filter with N taps, where N is the number of samples with which we reconstruct a synchrotron oscillation.

The output signal is computed as the convolution sum of N preceding values of the input signals $\Delta\varphi_{n-i}$

$$y(t_n) = G \sum_{i=1}^{N} \Delta\varphi(t_{n-i}) h_i \ , \tag{24}$$

where h_i are the filter coefficients and G is the feedback gain.

As shown in the simulations, the feedback system performs satisfactorily with a number of taps as small as 5. A preliminary estimate of the number DSP's needed for 30 bunches is $\sim$ 5, assuming a DSP with an instruction time of 25 ns. Different filter algorithms were also investigated and the best effectiveness is achieved with sinusoidal and high-pass configurations.

The proposed architecture of the digital part exhibits good flexibility together with reasonable hardware complexity.

5.4 *Longitudinal kicker*

The energy correction in terms of the output power P_{fb} of the final amplifiers is

$$\Delta U_{fb} = \sqrt{2 P_{fb} (RT^2)_k} \tag{25}$$

where $(RT^2)_k$ is the kicker shunt impedance, corrected by the transit time factor. The bandwidth of the kicker must be at least half the bunch frequency in order to kick all bunches separately.

In order to reduce the power requirements of the final feedback amplifiers and the reflections due to mismatches at the power port, we are optimizing the design of the longitudinal kicker. The present choice is a series of two $\lambda/4$ strip lines with full coverage, connected with $\lambda/2$ delay lines. This arrangement provides a peak shunt impedance of $\sim$ 400 Ω and a half-power bandwidth in excess of 1/2 the maximum bunch frequency.

From the simulation results, the power needed to damp the bunch oscillations with a maximum time displacement equivalent to the bunch length ($\sim$ 100 ps), as is expected at the injection, is less than 500 W.

6 TIME DOMAIN SIMULATION CODE

The theoretical analysis presented in section 2 considers the coupling of a single sideband with a single parasitic resonance of the RF cavity. The bunches are assumed to be equally populated and spaced.

However it is not practical to analytically study the beam dynamics under the conditions of unequally spaced and unequally populated bunches, nor for large oscillations at injection and under the effect of the bunch-by-bunch feedback. These different scenarios are better investigated by means of a properly developed time domain simulation code.

6.1 The algorithm

The core of the algorithm can be divided into the propagation around the ring, the feedback effect, and the beam-cavity interaction.

To describe the motion of a single bunch in the machine, we use the energy deviation ΔE and the phase $\Delta\varphi$.

In the propagation around the ring, each bunch loses energy due to the broad band impedance (U_{bb}) that does not depend on the energy of the bunch, and to synchrotron radiation (U_r), for which we use the following linear expression,

$$U_r = U_o\left(1 + 2\frac{\Delta E}{E}\right), \tag{26}$$

where U_o is the energy lost by a synchronous particle.

It is therefore possible to correlate the quantities ΔE and $\Delta\varphi$ just outside the RF cavity with those we find at the entrance of the feedback kicker at the following turn:

$$\begin{pmatrix}\Delta E\\ \Delta\varphi\end{pmatrix}_K = \begin{pmatrix}1-2\frac{U_o}{E} & 0\\ \frac{2\pi h\alpha_c}{E} & 1\end{pmatrix}\begin{pmatrix}\Delta E\\ \Delta\varphi\end{pmatrix}_{\mathrm{rf}} - \begin{pmatrix}U_o + U_{bb}\\ 0\end{pmatrix}, \tag{27}$$

where α_c is the momentum compaction, h is the harmonic number, the subscript k indicates at the entrance of the kicker, and the subscript rf indicates a location outside the RF cavity.

All parts of the feedback system described in Section 5 are simulated. It is possible to change the system configuration and the feedback gain by means of the input file. Different digital filters such as delay lines, high and low pass, derivative and sinusoidal filters have been investigated also.

The cavity is simulated as a series of parallel RLC circuits that represent the HOMs. When a charge q_b crosses the cavity, it perturbs the voltage of each mode. In the simulations we have assumed the fundamental-mode to be perfectly compensated, that is,

$$V_g = \hat{V}_g\ \cos(\Delta\varphi)\ , \tag{28}$$

with $\hat{V}_g$ the peak cavity voltage.

The induced voltage for each mode is a kick ΔV depending on the shunt resistance R and the quality factor Q of that mode. In order to take into account the bunch length (we assume that the bunch has a Gaussian distribution), the shunt resistance is corrected by the factor $\exp\left[-(\omega_r\sigma_t)^2\right]$.

The behavior of the induced wake voltage of each mode is described by means of a propagation matrix for the conjugated variables $v(t)$ and $i(t)$. Between the passage of two bunches, the voltage of each mode executes free oscillations represented by the homogeneous solution of the differential equation of an RLC parallel circuit. Therefore we have[26,27]

$$\begin{pmatrix} v(t) \\ i(t) \end{pmatrix} = \exp(-\alpha_f t) \begin{pmatrix} \cos(\beta t) - \frac{\alpha_f}{\beta} \sin(\beta t) & -\frac{\omega_r R}{\beta Q} \sin(\beta t) \\ \frac{\omega_r Q}{\beta R} \sin(\beta t) & \cos(\beta t) + \frac{\alpha_f}{\beta} \sin(\beta t) \end{pmatrix} \begin{pmatrix} v(t_o) \\ i(t_o) \end{pmatrix}, \tag{29}$$

where β is the natural angular frequency and $v(t_o)$ and $i(t_o)$ are the starting conditions.

When a bunch crosses the cavity, we increase $v(t)$ by the kick ΔV and continue the propagation. The total energy gained by the bunch in the RF cavity is therefore

$$E_c = e \left(V_g + \sum_{\text{all the HOMs}} \left[v(t) + \frac{1}{2} \Delta V \right] \right), \tag{30}$$

where the last term takes into account the fundamental theorem of beam loading: a bunch sees half of the wake voltage it induces during its passage.

6.2 *Application to* DAΦNE

We have performed different simulations with all the HOMs measured values of the waveguide loaded cavity as given in Table 3.

Since the frequency may vary during the machine operation, we have chosen to simulate the worst case, i.e., all the HOMs are in full coupling with the unstable sidebands of the beam spectrum.

First, we have observed the instabilities with the feedback off by simulating the injection of the 30th bunch (with an error of 100 ps) assuming all the others to be in the equilibrium state. Figure 8 shows the oscillations of a perturbed bunch, and Figure 9 the oscillations of the injected bunch, during the first 5000 turns. Then we have found a feedback configuration such as to damp the oscillations with a kicker voltage of 400 V, as we can see in Figures 10 and 11.

To be sure that the injection of the 30th bunch was the most dangerous from the stability point of view, with the same feedback parameters we simulated the injection of the nth bunch with $n - 1$ bunches already at the equilibrium phase. In Figure 12 we show the maximum phase excursion of the bunch versus the number of the bunch. As expected, the oscillations become larger when we increase the total current stored.

The code has been recently improved[28] by including the effects of the time evolution of the fundamental-mode voltage due to the beam loading and to an RF feedback system.

7 CONCLUSIONS

Multibunch instabilities are certainly one of the main problems to solve in reaching a very high luminosity in DAΦNE. We made a strong effort on the analysis of the methods that

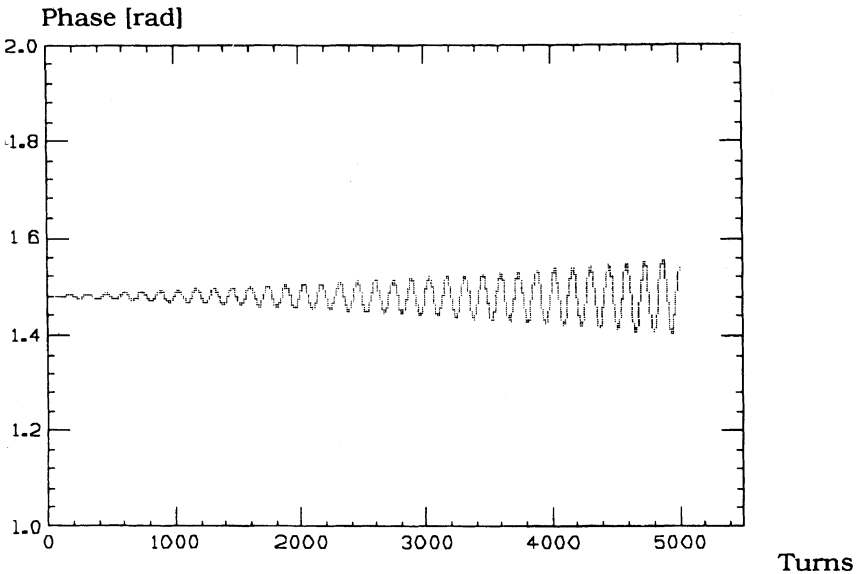

FIGURE 8: Oscillations of a perturbed bunch.

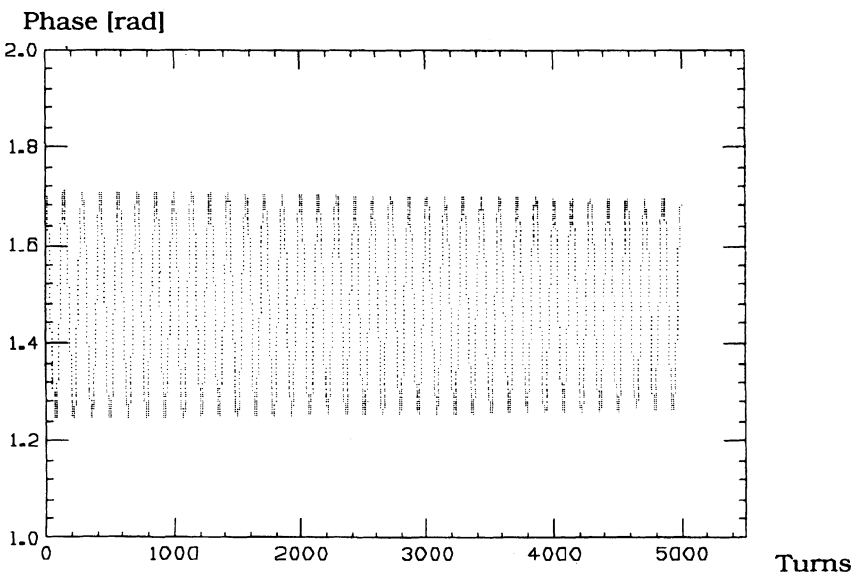

FIGURE 9: Oscillations of the injected bunch.

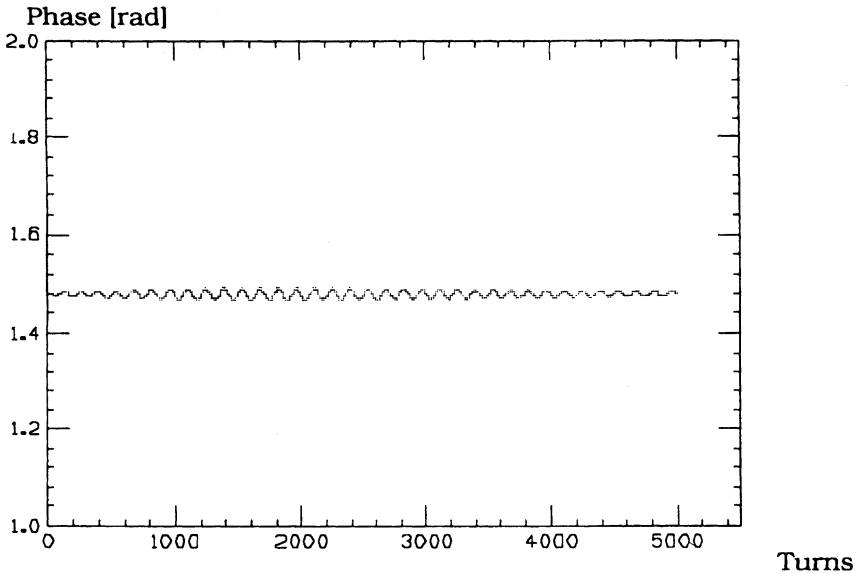

FIGURE 10: Oscillations of a perturbed bunch with the feedback on.

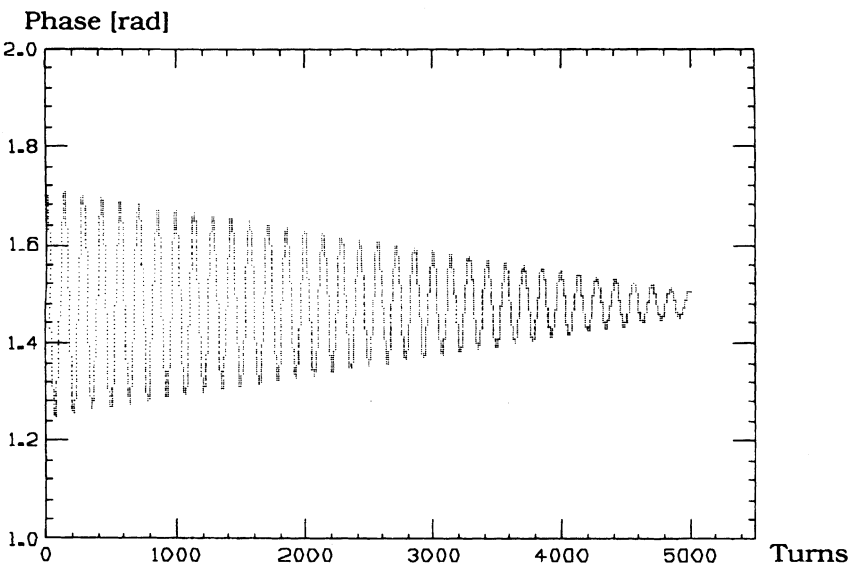

FIGURE 11: Oscillations of the injected bunch with the feedback on.

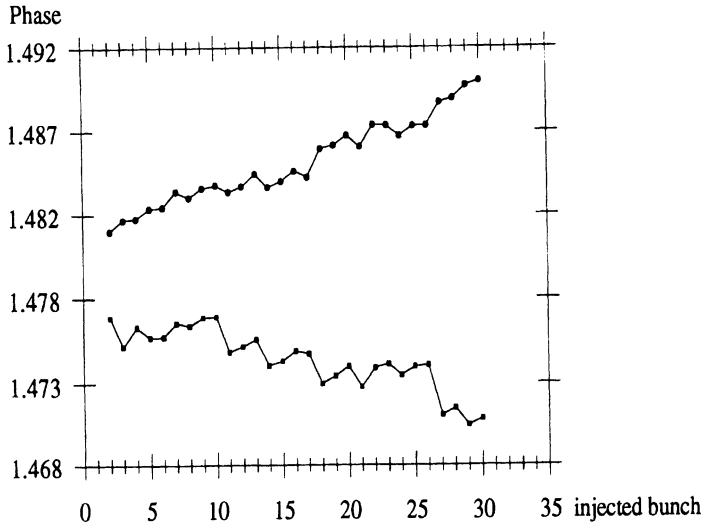

FIGURE 12: Maximum perturbation of the stored bunches.

could take these instabilities under control. We are reasonably confident that by properly damping the resonant fields in the machine, we will be able to damp the residual instability by means of a feedback system.

ACKNOWLEDGEMENTS

We are pleased to acknowledge the collaboration and the hospitality provided to some of us by all the members of PEP-II group, in particular John Fox and Gerard Oxoby. We also like to thank Bruno Zotter and Albert Hofmann for the very useful discussions and suggestions on the subject of this paper.

REFERENCES

1. G. Vignola, DAΦNE: the Frascati Φ-Factory, in Proceedings of the 1991 IEEE Particle Accelerator Conference, (San Francisco, 1991) vol. 1, pp. 68–70.
2. F. Sacherer, IEEE Trans. Nucl. Sci. **NS-24**, 1393 (1977) also CERN/PS-BR/77 5 and 6.
3. J. L. Laclare, CERN 87–03 (1987) vol. I, pp. 264–326.
4. M. S. Zisman *et al.*, LBL 21270.
5. A. Hofmann *et al.*, IEEE Trans. Nucl. Sci. **NS-26**, 3514 (1979).
6. A. Massarotti, *et al.*, Particle Accelerators, **35**, 167–175 (1991).
7. N. Kroll and D. Yu, Particle Accelerators, **34**, 231–250 (1990).
8. P. Arcioni and G. Conciauro, Particle Accelerators, **36**, 177–203 (1991).
9. An Asymmetric B-Factory, LBL PUB-5303.

10. H. Hindi *et al.*, Down sampled signal processing for a B Factory bunch-by-bunch feedback system, Proceedings of the 1992 European Particle Accelerators Conference (Berlin, 1992) pp. 1067–1069.
11. J. D. Fox *et al.*, Feedback Implementation Options and Issues for B Factory Accelerators, SLAC-PUB-5932 (1992).
12. D. Briggs *et al.*, Computer modeling of bunch-by-bunch feedback for the SLAC B-Factory design, IEEE Particle Accelerator Conference, San Francisco (1991).
13. K.A. Thompson, Simulation of longitudinal coupled-bunch instabilities, SLAC technical note ABC-24 (1991).
14. A. Hofmann and B Zotter, private communication.
15. M. Migliorati and L. Palumbo, Multibunch Instabilities in DAΦNE: longitudinal and transverse coherent frequency shift, DAΦNE Technical Note G-18 (1993).
16. M. Bassetti *et al.*, A Time Domain Simulation Code of the Longitudinal Multibunch Instabilities, DAΦNE Technical Note G-19 (1993).
17. T. Weiland, Nucl. Instrum. Meth. **216** (1983), pp. 329–348.
18. T. Weiland, Single Mode Cavities, DESY Report 83/073 (1983).
19. T. Weiland, NIM, **212** (1983), pp. 13–34.
20. S. Bartalucci, *et al.*, A low loss cavity for the DAΦNE Main Ring, DAΦNE Technical Note G-6, (1991).
21. P. Fernandes and R. Parodi, IEEE Trans. Magn. **21** (6) (1985), 2246.
22. R. Rimmer *et al.*, An rf Cavity for the B-Factory, SLAC-PUB-6129, (1993).
23. R. Collin, Field Theory of Guided Waves (McGraw-Hill, New York, Toronto, London, 1960).
24. R. Boni *et al.*, Study of parasitic mode absorbers for the Frascati Φ-Factory rf cavities, LNF-93/014 (P), (1993).
25. R. Boni *et al.*, A broadband waveguide to coaxial transition for high order mode damping in particle accelerator rf cavities, submitted to Particle Accelerators.
26. M. Bassetti, Finite difference equations calculations of beam-cavity coupling instability, LNF Note 67/45, Frascati (1967).
27. M. Migliorati, dissertation, Roma, 1992.
28. A. Gallo *et al.*, Time domain simulation of DAΦNE rf feedback, DAΦNE Technical Note, in preparation.